Journal of Applied Polymer Science

Morphology and Properties of Polystyrene/Agave Fiber Composites and Foams

Francisco Javier Moscoso,[1] Liliana Martínez,[1] Gonzalo Canche,[2] Denis Rodrigue,[3] Rubén González-Núñez[1]

[1]Centro Universitario de Ciencias Exactas e Ingeniería, Universidad de Guadalajara, Guadalajara, Jalisco 44430, México
[2]Centro de Investigaciones Científicas de Yucatán, Mérida, Yucatán 97200, México
[3]CERMA, Laval University, Quebec City, Quebec G1V 0A6, Canada

Correspondence to: R. González-Núñez (E-mail: rubenglz@cencar.udg.mx)

ABSTRACT: In this work, agave fibers were blended with polystyrene to produce foamed and unfoamed composites. The effect of fiber size and density reduction on the morphological, thermal, mechanical, and rheological properties, as well as crystallinity and water absorption kinetics of the composites was assessed. The results show that Young's modulus and tensile strength increased with increasing fiber content, but decreased with density reduction. Increasing fiber content and decreasing the size of the fibers both increased crystallinity of the composites. Finally, water uptake and diffusion coefficient were found to increase with increasing fiber content for all sizes. © 2012 Wiley Periodicals, Inc. J. Appl. Polym. Sci. 000: 000–000, 2012

KEYWORDS: polystyrene; composites; morphology; mechanical properties

Received 18 March 2011; accepted 30 March 2012; published online
DOI: 10.1002/app.37843

INTRODUCTION

Polymer composites have been studied in great details in the scientific literature, as well as in several industrial applications.[1–9] More recently, composites reinforced with natural fibers received a special attention in view of using natural resources for commercial applications. The main advantages of these materials are lower costs, higher specific mechanical properties (per unit weight), and reinforcement based on renewable alternatives. Nowadays, a wide variety of natural fibers are used as reinforcement or fillers. For example, cotton, jute, and flax are vegetable fibers most commonly used to reinforce polymers such as polystyrene, polyester, polyolefin, and epoxy resins due to their availability and good specific properties.[3–6] One particular fiber that has received attention, especially in Mexico, is the agave fiber (*Agave Tequilana Weber Azul*) which is a residue of the tequila industry. The production of Tequila in Mexico was 250 million of liters in 2010 from about one million of tons of Agave fiber. This fiber represents a major problem over the years since most of these fibers are burned onsite. This waste can be revalorized and used in an environmentally friendly polymer composite.[7,8,10,11]

When using natural fibers, several aspects of the final composites must be determined. The effect of processing method (thermomechanical history) and fiber dimensions are important to obtain better mechanical properties.[6,7] Also, moisture content is an important factor[8] and the effect of fiber content and sizes on the melt rheology of the polymers was also studied in relation with optimum processing conditions.[9,10] Surface modification of natural fibers using bacteria,[12] chemicals,[13,14] or adding coupling agents in the composite[15] was found to improve adhesion and dispersion, since the main drawback associated with natural fibers in most polymer composites is poor interfacial bonding due to weak compatibility and dispersion of hydrophobic cellulosic fibers inside hydrophobic polymer matrices.[16–19]

More recently, several ways to decrease the weight of molded parts were investigated, especially for packaging and transport applications. To this end, polymer foams were developed by introducing a foaming agent (chemical or physical) while processing.[20–22] This also led to the development of a new class of materials: polymer composite foams.

Although several works can be found for different polymer/fiber combinations, very few studies were devoted to polystyrene foams reinforced with natural fibers. Only, Doroudiani and Kortschot,[23] as well as Rizvi et al.[24] used wood fibers, while Mihai et al.[25] used starch.

Based on the limited amount of information available in the literature, the goal of this work is to investigate the effect of

natural fiber addition in polystyrene. In particular, the effect of fiber dimension and content, as well as density reduction through foaming, are studied in relation with changes in morphological, mechanical, rheological, thermal, and water absorption kinetics. As a first step, no modification of the agave fiber or coupling agent was used to produce the composites.

EXPERIMENTAL

Materials

The polymer matrix used was polystyrene (PS) HF555 from Industry RESIRENE (Mexico). This polymer has a melt index of 16 g/10 min and a density of 1.05 g/cm^3. The average molecular weight of PS was determined (obtained $M_w = 258{,}416$ Dalton with polydispersity = 1.54) using a Waters 24114 gel permeation chromatograph (GPC) equipped with a refractive index detector 515. Chromatographic grade tetrahydrofuran (Aldrich) was used as the mobile phase. Foaming was performed using azodicarbonamide (ACA) from Aldrich Chemicals (St. Louis, MO) with 99% purity. As reinforcement, agave fibers (*Agave Tequilana Weber Azul*) were obtained as a residue of the regional tequila industry (Jalisco, Mexico).

Preparation of Agave Fibers

The agave fibers were first washed five times with water at 40°C and dried at room temperature. They were then grinded and sieved by a Ro-tap RX-29 mechanical sifter with different Tyler screens according to ASTM E-11. Only selected sizes were kept to study the effect of fiber dimensions: 60–80, 80–100, and 120–140 mesh. Finally, the fibers were dried 24 h in an oven at 80°C to eliminate moisture before incorporation in the PS matrix.

Foamed and Unfoamed Composites

Compounding was done in a Leistritz twin-screw extruder model Micro 27 GL/GG 32 D. The temperature profile from the feed hopper to the die was controlled at: 170, 170, 180, 180, 185, 185, 190, 190, and 190°C. Overall, three agave concentrations were produced: 10, 20, and 30% by weight. The screw speed was set at 100 RPM giving a total flow rate of 4 kg/h. The die was cylindrical with a diameter of 2 mm. For foaming, the same compounds were produced by adding 1% by weight of ACA. Finally, the blends were pelletized and the material was introduced in a compression molding press with a mold having dimensions of 20 × 20 × 0.3 cm^3. Pressing was done at 190°C with a pressure of 0.5 MPa for 20 min. Foaming was obtained by slightly opening the mold before starting the cooling cycle using forced air convection.

Morphology

Rectangular samples of 1.0 × 5.0 × 0.3 cm^3 were cut directly from the molded plates and dipped in liquid nitrogen before being cryo-fractured. The morphology of the foams and composites were obtained via a digital table top microscope HITACHI model TM-1000. The micrographs were quantitatively analyzed using the Image Pro Express 4 software, for deformed particles is possible to measure the periphery (p) of the cell and the area (A). With these values, an average diameter (d) is obtained from $A = \pi(d/2)^2$. The same equipments were used to measure fiber dimensions. In each case (fibers and cells), a minimum of 50 particles are used to get the average and standard deviation.

Mechanical Testing

Tensile testing of the foamed and unfoamed composites was carried out according to ASTM D-638. Type IV dog bone sample were die cut directly in the molded plates and tested on a TDCC-20 Physical Test Solutions universal testing machine. The crosshead speed was 2 mm/min tensile modulus, tensile strength and elongation at break were obtained from the stress–strain curves at room temperature. The data reported are the average and standard deviation of at least 10 samples.

Rheological Testing

The melt viscosity of the compounds was characterized using a Rosand double-bored capillary rheometer model Rh-2000. All the measurements were performed at 190°C over a range of deformation velocities to get the viscosity-shear rate curves.

Adsorption Isotherms

Nitrogen adsorption isotherms (BET method) were done to characterize the specific surface areas of the fibers. The measurements were done at 77 K on a Micromeritics ASAP 2405 equipment. The pore size distribution was calculated following the method developed by Barrett, Joyner and Halenda (BJH method).[26]

Thermal Analysis

Thermogravimetric analysis (TGA and DTGA) were obtained with a thermobalance TGS-7 from Perkin Elmer. Heating rate of 10°C/min was applied for a temperature range between 50 and 700°C under a nitrogen atmosphere. Also, differential scanning calorimetry (DSC) experiments were carried out on a Perkin-Elmer DSC Pyres 6. Each sample went through a programmed heating profile between 30 and 200°C at rate of 10°C/min. The glass transition temperature (T_g) was determined for the neat polystyrene, the foams, and the composites.

Raman Spectroscopy

Raman spectra were taken with a model R-2001 from Raman systems. Raman spectroscopy is a nondestructive technique which does not need any sample preparation requirement.[27] This technique was used to determine crystallinity of the composites foamed, unfoamed, and neat material.

Water Absorption

Rectangular specimens having 5 cm in length, 1 cm in width, and 0.3 cm in thickness were cut from the molded plates. Water adsorption experiments were carried out as described in ASTM D-570. Three specimens were selected for each composition and dried in an oven for 24 h at 80°C. Once dried, the samples were weighed and immersed in a water bath containing distilled water at 25°C. The tests were performed for a total duration of 568 h. During this period, the samples were removed at regular interval, wiped with a filter paper to remove surface water and weighed. The samples were then returned to the water bath to pursue the water adsorption test. The water uptake (M%) during the absorption was determined as:

$$M\% = \frac{(\mathrm{M_t} - \mathrm{M_i})}{\mathrm{M_i}} 100 \quad (1)$$

where M_i is initial weight of the dry sample and M_t is the weight of sample with moisture at a given time.

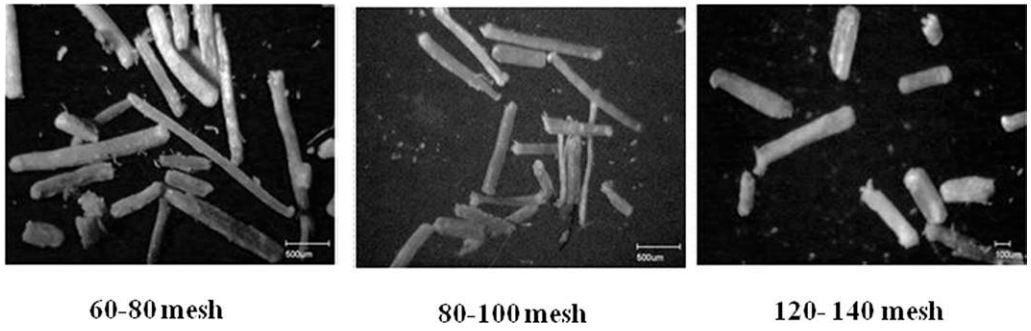

Figure 1. Typical micrographs of the original agave fiber (before processing).

RESULTS AND DISCUSSION

Morphology

Figure 1 shows typical micrographs of the original agave fiber (before processing). From the micrographs, the length over diameter ratio (*L/D*) value of the fibers was determined by taking measurements of 100 fibers. On the basis of the results, the average and standard deviations were determined as 6.02 ± 0.50 for 60–80 mesh, 5.68 ± 0.23 for 80–100 mesh, and 5.06 ± 1.04 for 120–140 mesh. This parameter is important since higher *L/D* ratio should have beneficial effect on final mechanical properties.[2]

Figure 2 shows some microphotography of the PS unformed [Figure 2(a)] and foamed at different compositions. Based on the image analysis, Table I presents the cell diameters obtained for the foams. It is clear that the average cell size decreases with increasing fiber content. It is known that the fibers can induce

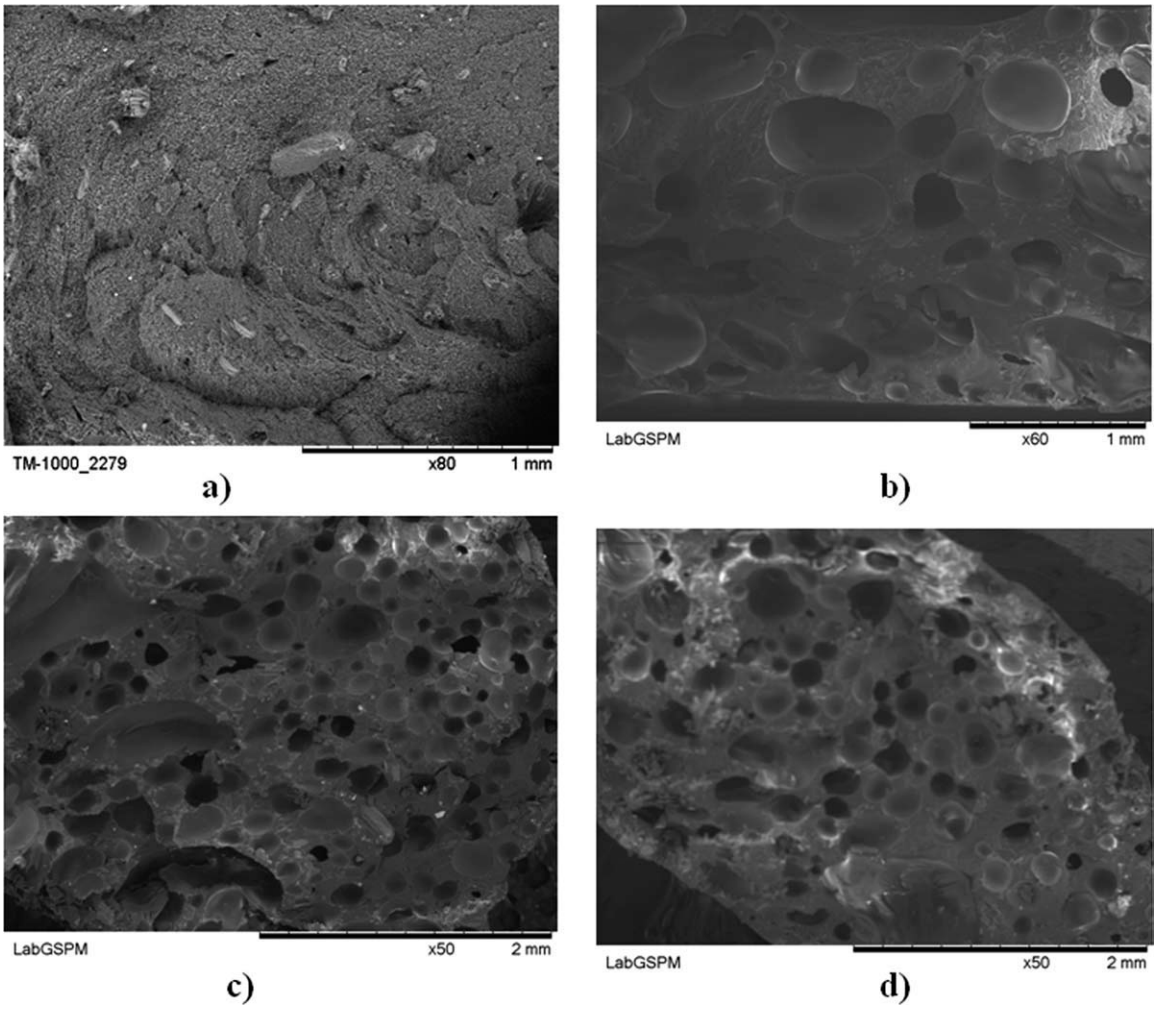

Figure 2. Typical micrographs of PS: 10% agave fiber unfoamed (a), foamed with different agave fiber contents: 0% (b), 10% (c), and 30% (d).

Table I. Average Foam Cell Sizes (μm)

Composition PS/agave	No fiber	60–80 mesh	80–100 mesh	120–140 mesh
100/0	228 ± 35	-	-	-
90/10	-	226 ± 63	220 ± 32	222 ± 39
80/20	-	187 ± 39	186 ± 33	185 ± 30
70/30	-	163 ± 38	166 ± 28	176 ± 29

heterogeneous nucleation in a foaming polymer, thus producing a higher number of cells.[28] Since more cells are created, the fixed amount of gas (1% ACA here) is consumed more rapidly and there is less possibility for cell growth. Additionally, poor bonding at the polymer-fiber interface may already induce gas pockets in the polymer melt leading to lower driving forces to create the foam cell.[29] Although fiber size did not influenced significantly the cell size distribution, increasing fiber content decreased cell size because the presence of more fiber creates more surface area for heterogeneous nucleation to occur.

Thermal Characterization of the Fibers

Figure 3 presents the thermogram (TGA) curves of materials pure and PS/agave fiber composites for the 60–80 mesh sizes. The presence of agave fiber changes the decompositions pattern of PS/agave fiber composites. For neat PS decomposition starts at 350°C and is complete at 450°C, which indicates a better thermal stability. In the case of PS/agave fiber there is slight decomposition about at 225°C and the main decomposition begins a higher temperature close to 400°C and the degradation is almost complete at a temperature of 470°C. It shows that the thermal stability of composite is higher. PS thermogravimetric scans from 50 to 300°C shows a thermal stability and not mass loss, whereas that of agave fiber have an initial loss of 12% between 50 and 150°C due to dehydration of fiber, then a main loss (around 55%) in the range 250–275°C due to thermal depolymerization of the hemicelluloses and rupture of glycosides groups of the cellulose which are the main components of the fibers. Finally, decomposition at temperatures higher than 400°C is attributed to the degradation of cellulose and lignin.[30–32]

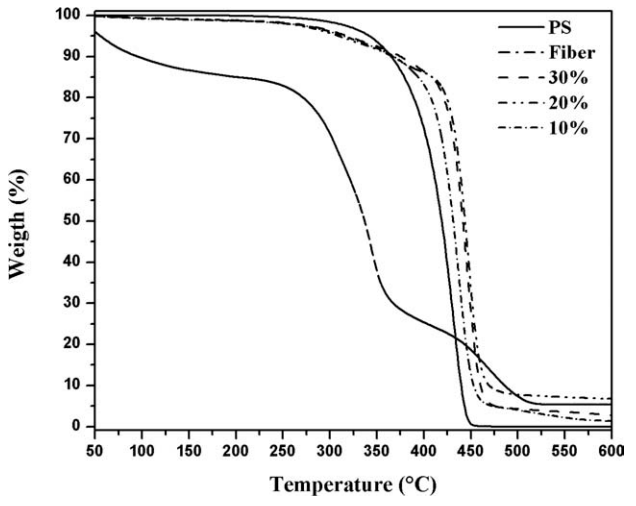

Figure 3. TGA curves of materials pure and PS/agave fiber composites (60–80 mesh).

Table II. Tensile Properties of Foamed and Unfoamed PS

ACA content (wt%)	Density (g/cm^3)	E (MPa)	σ (MPa)	ε_b (%)
0	1.09 ± 0.05	3499 ± 104	30 ± 9	1.19 ± 0.17
1	0.83 ± 0.04	2906 ± 167	28 ± 11	1.21 ± 0.20

Mechanical Characterization of the Composites

Based on the stress–strain curves obtained, Table II shows the Young modulus (E), tensile strength (σ), and deformation at break (ε_b) of the foamed and unfoamed PS matrix. Since all the materials were brittle, the tensile strength is equal to the stress at break. Table II also shows that the addition of only 1% of ACA produced a 24% reduction in density leading to a 17% decrease in modulus with negligible variation in strength and elongation at break within experimental uncertainty.

Table III shows the tensile properties of all the composites produced to determine the effect of fiber content, fiber size, and density reduction. First, increasing fiber loading improves substantially the tensile modulus and strength of the foamed and unfoamed composites. As the fiber concentration increases, the stress is more evenly distributed and the strength of the composite increases. As proposed by Nair Madikandan and Thomas,[18] if the fibers are oriented perpendicularly to the direction of the crack propagation, the crack can be hindered and this accounts for the increase in tensile strength and modulus. Table III also shows that increasing fiber size (decreasing mesh) produced stronger foamed and unfoamed materials (higher modulus and strength). As expected, density reduction led to lower modulus and strength since less material is available to sustain the applied stresses. Finally, since all the materials are very brittle with less than 2% elongation at break, the latter was not significantly affected by the fibers and cells for all the conditions tested.

Rheology

From the data obtained on the capillary rheometer (shear rate ranges between 10 and 1000 s^{-1}) polymer melts and composites have a shear-thinning (pseudoplastic with $n < 1$) behavior usually described by the simple power-law model[33,34]:

$$\eta = m\dot{\gamma}^{n-1} \tag{2}$$

where m and n are the consistency and power-law index, respectively. Table IV presents the results for the PS/agave fiber composites. The presence of fiber in polymer melts perturbs the normal flow of the polymer.[33] The consistency index (m) is function (increase) of fiber content, while power-law index (n) decrease with fiber content (see Table IV). This combined effect produces a slight diminution of viscosity. However, increasing fiber content leads to more hydrodynamic resistance to bubble growth, thus smaller cells are observed as fiber content increases.

Porosity

The BET measurements were performed only for the composite with the highest amount of fiber (30%), but for all sizes

Table III. Tensile Properties of PS/agave Fiber Composites

	60–80 mesh			80–100 mesh			120–140 mesh		
Fiber content (%)	*E* (MPa)	σ (MPa)	ε_b (%)	*E* (MPa)	σ (MPa)	ε_b (%)	*E* (MPa)	σ (MPa)	ε_b (%)
Foamed									
30	4740 ± 273	60 ± 10	1.34 ± 0.26	4573 ± 234	47 ± 14	1.32 ± 0.26	4022 ± 126	46 ± 15	1.32 ± 0.23
20	4021 ± 192	48 ± 12	1.28 ± 0.25	4010 ± 198	42 ± 10	1.30 ± 0.20	3643 ± 96	40 ± 17	1.24 ± 0.25
10	3527 ± 108	33 ± 9	1.23 ± 0.22	3481 ± 167	38 ± 8	1.25 ± 0.23	3538 ± 108	37 ± 12	1.21 ± 0.16
Unfoamed									
30	4929 ± 148	62 ± 15	1.35 ± 0.29	4831 ± 130	44 ± 14	1.35 ± 0.26	4226 ± 86	42 ± 7	1.35 ± 0.26
20	4105 ± 116	49 ± 10	1.28 ± 0.24	3898 ± 265	42 ± 9	1.22 ± 0.17	3739 ± 72	31 ± 10	1.23 ± 0.23
10	3813 ± 156	44 ± 13	1.22 ± 0.19	3525 ± 189	38 ± 12	1.22 ± 0.13	3345 ± 48	30 ± 12	1.20 ± 0.19

(60–80, 80–100, and 120–140 mesh). Figure 4 shows the nitrogen adsorption the shape isotherms at 77 K, the shape of the isotherms correspond to the Type II and exhibit hysteresis loops of H1 type according to the IUPAC classification,[35] typical of materials agglomerates or compacts of spheroidal particles of fairly uniform size and array. At low relative pressure formation of a monolayer of adsorbed molecules is the prevailing process, while at high relative pressure a multilayer adsorption takes place.[36,37] Size mesh 60, 80, and 120 adsorbents share these overall features but differ when their isotherms. The slope of isotherm to low-pressure is different for each size mesh, this correspond to different areas obtained for each mesh of the macropores surface. Table V clearly shows that higher surfaces areas and smaller pore sizes are obtained as mesh size increases.

DSC Analysis

Changes in the PS glass transition temperature due to the presence of agave fibers were reported in previous studies.[38,39] For our samples, the T_g for all the composites and foams vary between 94.1 and 96.8 °C, while it is near 90°C for the neat foamed and unfoamed polystyrene. Nevertheless, the mesh size did not change significantly the T_g of the foamed and unfoamed composites as reported in Table VI. Also T_g slightly increased with fiber content as reported by Amash and Zuggenmaier.[40] Finally, the T_g of the foamed PS matrix was lower than its unfoamed counterparts, while the reversed is observed for the composites. This observation indicates that foaming and fiber addition are producing opposite effects on the resulting T_g of the materials.

Table IV. Power-Law Parameters for PS/Agave Fiber Composites at 190°C

Fiber content (%)	*m* (kPa.s^n)	*n* (-)
0	11.0	0.369
60-80 mesh		
30	14.8	0.270
20	11.4	0.349
10	8.81	0.393
80-100 mesh		
30	15.2	0.300
20	13.2	0.328
10	11.7	0.377
120-140 mesh		
30	13.2	0.329
20	10.5	0.381
10	9.36	0.395

Raman Spectroscopy

Raman spectroscopy can be used to determine crystallinity as described by Torres et al.[41] Syndiotactic polystyrene has been found to exhibit two distinct vibrational peaks in the Raman spectrum corresponding to the vibrational mode. The peaks of Raman α/β crystalline forms were determined for the studied range to be: 2845, 990, 772, 526, and 452 cm^{-1}. Figure 5 shows the Raman spectrum of the composites for the 60–80 mesh agave fibers. The plots present the characteristic peaks of α and β crystalline phase of syndiotactic polystyrene for the composites. Determination of crystallinity was proposed by Kellar et al.[42,43] and the amount of crystallinity (X_c) can be calculated as:

$$X_c = \frac{I_{773} - I_{777}^{\text{melt}}}{I_{773} + I_{796}} \quad (3)$$

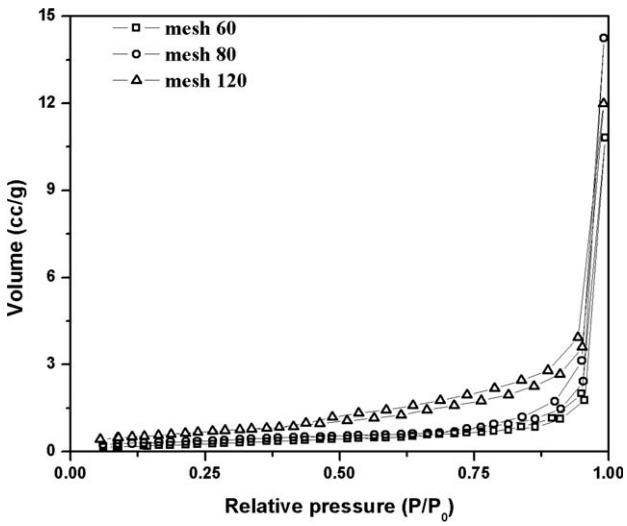

Figure 4. Adsorption/desorption isotherm with 30% agave fiber for all sizes.

Table V. Porosity Characterization of the Composites with 30% Agave Fiber

Fiber size (mesh)	Area (m^2/g)	Pore diameter (Å)
60-80	0.695	2560
80-100	1.30	2190
120-140	2.39	2010

where 777 cm^{-1} is a residual component of all-trans conformations within the amorphous materials, 773 cm^{-1} is the relative integrated area of the all-trans conformations and 796 cm^{-1} is the total integrated intensity of the amorphous non-trans sequences. The crystallinity (%) calculated by Raman spectroscopy ($\%_{773}$) is thus given by:

$$\%_{773} = 100X_c \quad (4)$$

and the values are presented in Table VI. It is clear that the composites have higher crystallinity for both foamed and unfoamed materials. This behavior is attributed to the presence of agave fibers acting as nucleating agents for crystallization. Similar behaviors for other cellulose based composites have been reported by Joseph et al.,[39] Ishida and Bussi,[44] and Sun et al.[45] using DSC data for crystallinity determination. As for the T_g results, crystallinity increases with fiber content, but negligible differences are seen between foamed and unfoamed samples for all mesh sizes and fiber contents.

Water Absorption

Figure 6 shows the experimental water absorption curves for the foamed and unfoamed composites prepared with the 60–80 mesh agave fibers. From this figure, it is clear that increasing fiber content increases water uptake and Table VII reports the equilibrium values (M_∞). Mishra and Verma[46] and Tajvidi et al.[47] suggested that this is due to the increase number of free OH groups of cellulose at higher fiber content. These free OH groups come in contact with water and form hydrogen bonding, which results in weight gain in the composite. Also, since the tests were performed in immersion, the foams absorbed much higher quantities of water which is accumulated in the cells.

On the basis of the data of Figure 6, the diffusion coefficient (D) can be determined by the method described by Crank as[48]:

$$\frac{M_t}{M_\infty} = 1 - \frac{8}{\pi^2}\sum_{n=0}^{\infty}\frac{1}{(2n+1)^2}\exp(-D(2n+1)^2\pi^2 t/l^2) \quad (5)$$

where M_t is the mass of water absorbed in the sheet at time t, M_∞ is the mass of water absorbed at equilibrium, and l is the thickness of sheet. Figure 6 also shows that eq. (5) is in good agreement with the experimental data.

Table VII presents the diffusion coefficient obtained for all the foamed and unfoamed composites produced. In general, the diffusion coefficient follow a linear relationship with fiber content, this behavior was reported by Rao et al.[49] for a Jute-Epoxy composite. However, the effect of foaming and fiber size is unclear as reported in similar studies.[50,51] One explanation, as proposed by Wang et al.,[52] is that the diffusion theory does apply for mass transfer in complex systems like polymer composites. Another explanation is related to the morphology of the material. Since natural fibers and polymer matrices exhibit very different properties in terms of moisture absorption, the fiber distribution in the polymer matrix is a key parameter to the overall moisture absorption, especially when a third phase is present like in the foams. Nevertheless, more work will be needed to fully understand the complex relations between mass transfer, morphology and basic properties of each constituent.

CONCLUSIONS

In this work, agave fiber/PS composites were manufactured by compression molding. As a first step towards our understanding of complex polymer composites systems, the effect of fiber content and fiber sizes were studied for foamed and unfoamed materials. From the materials obtained, morphological, rheological, thermal, mechanical, and water absorption properties were determined. On the basis of the results obtained, several conclusions can be made for this system.

In general, increasing fiber content increase tensile modulus and strength, crystallinity, water uptake, and diffusion coefficient, as well as melt viscosity. On the other hand, increasing fiber content decreased cell size. As for fiber size, its effect on cell size, tensile elongation at break, crystallinity, water uptake, diffusion coefficient, and viscosity was found to be negligible for the

Table VI. Glass Transition Temperature (T_g) and Raman Crystallinity (X_c) of PS/Agave Fiber Foams and Composites

Fiber content (%)	ACA content (%)	T_g (°C)	X_c (%)
0	0	90.1	4.48
0	1	87.2	4.40
60-80 mesh			
30	0	95.9	8.51
20	0	94.6	7.22
10	0	94.1	5.83
30	1	95.6	9.19
20	1	95.0	8.01
10	1	95.8	5.44
80-100 mesh			
30	0	96.8	11.1
20	0	95.7	7.80
10	0	95.4	6.30
30	1	96.5	9.28
20	1	95.6	7.71
10	1	94.8	5.50
120-140 mesh			
30	0	96.6	11.4
20	0	96.5	8.02
10	0	96.2	6.18
30	1	96.2	11.5
20	1	95.5	8.04
10	1	94.2	6.00

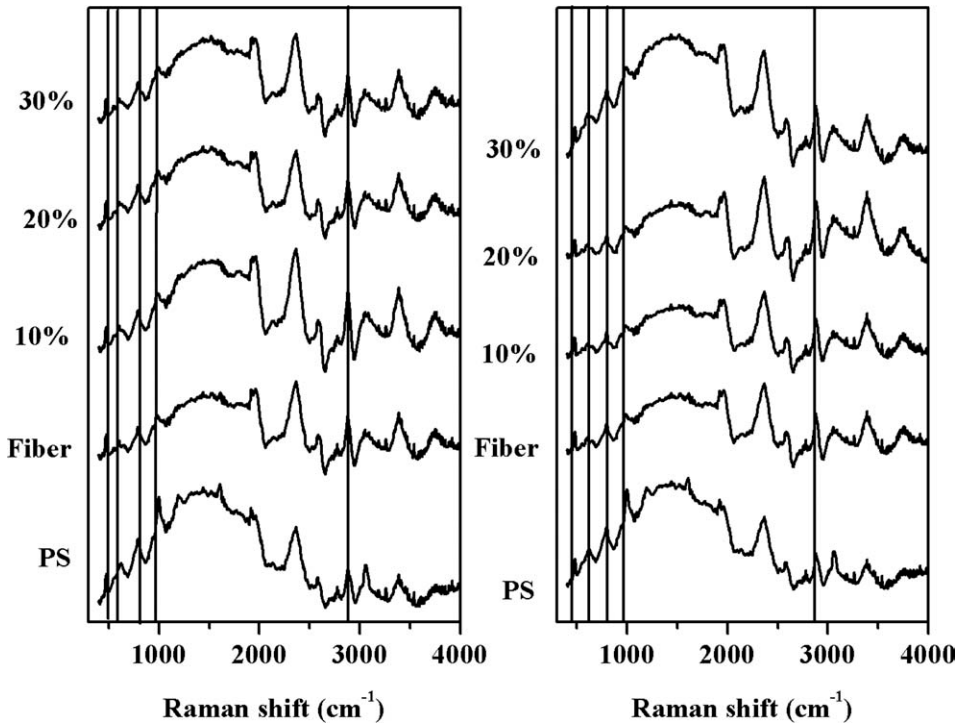

Figure 5. Raman spectra for the foamed (right) and unfoamed (left) PS/agave fiber composites (60–80 mesh).

range of parameters studied. This may be related to the fact that the size of the fibers changed (60–140 mesh), but the length/diameter ratio did not (between 5 and 6 only). Finally, density reduction through foaming decreased tensile modulus and strength, but substantially increased water uptake. Nevertheless, the complex interactions between morphology and mass transfer must be further studied in order to improve our understanding of water absorption of natural fiber reinforced polymer composite foams.

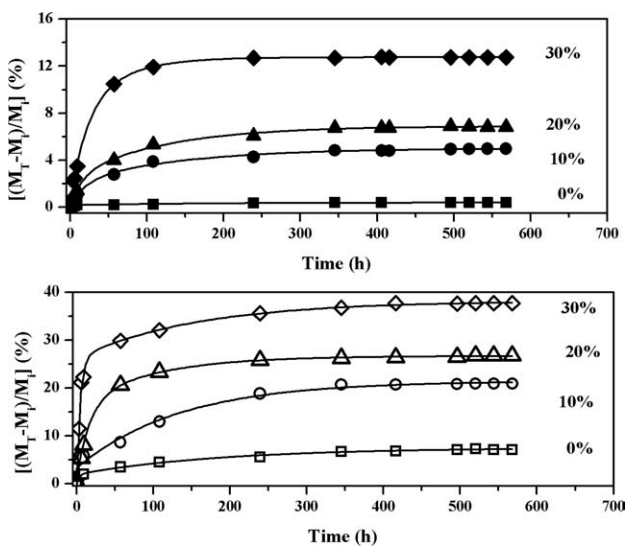

Figure 6. Water absorption curves for the unfoamed (top) and foamed (bottom) PS/agave fiber composites (60–80 mesh).

Table VII. Water Diffusion Coefficient (D) and Maximum Water Uptake (M_∞) for PS/Agave Fiber Foams and Composites

Fiber content (%)	ACA content (%)	D (10^{-12} m^2/s)	M_∞ (%)
0	0	0.95	0.34
0	1	0.98	7.14
60–80 mesh			
30	0	4.33	12.7
20	0	2.94	6.83
10	0	2.40	4.91
30	1	4.71	37.8
20	1	3.73	26.8
10	1	2.27	21.1
80–100 mesh			
30	0	4.94	12.8
20	0	2.84	7.77
10	0	2.32	4.32
30	1	3.11	36.6
20	1	2.06	28.6
10	1	1.61	20.1
120–140 mesh			
30	0	4.18	10.7
20	0	3.83	5.62
10	0	3.46	3.92
30	1	3.24	38.0
20	1	2.32	28.1
10	1	2.31	20.1

ACKNOWLEDGMENTS

Financial support from Groupe de Travail Québec-Mexico (GTQM 2009-2011) and CONACyT (Mexico) are acknowledged for this work.

REFERENCES

1. Matuana L. M.; Balatinecz, J. *J. Polym. Eng. Sci.* **1998,** *38*, 765.
2. Migneault, S.; Koubaa, A.; Erchiqui, F.; Chaala, A.; Englund, K.; Wolcott, M. P. *Compos. Part A* **2009,** *40*, 80.
3. Plackett, D.; Jankova, K.; Egsgaard, H.; Hvilsted, S. *Biomacromolecules* **2005,** *6*, 2474.
4. Nishino, T.; Noriko, N. *Biomacromolecules* **2007,** *8*, 2712.
5. Chen, F.; Liu, L.; Cooke, P. H.; Hicks, K. B.; Zhang, J. *J. Ind. Eng. Chem. Res.* **2008,** *47*, 8667.
6. Sun, X.; Li, H.; Zhang, X.; Wang, J.; Wang, D.; Yan, S. *Macromolecules* **2006,** *39*, 1087.
7. Coutinho, F. M. B.; Costa, T. H. S.; Suareza, J.; Carlos, M.; Meloa, D. P. *Polym. Test.* **2000,** *19*, 625.
8. Álvarez, V. A.; Fraga, A. N.; Vázquez, A. *J. Appl. Polym. Sci.* **2004,** *91*, 4007.
9. Prasantha, K. R.; Manikandan, N. K. C.; Thomas, S.; Schit, S. C.; Ramamurthy, K. *Compos. Sci. Technol.* **2000,** *60*, 1737.
10. Leduc, S.; Galindo-Ureña, J. R.; González-Núñez, R.; Quirarte, J. R.; Riedl, B.; Rodrigue, D. *Polym. Polym. Compos.* **2008,** *16*, 115.
11. Gómez, D. M.; Galindo, J. R.; González-Núñez, R.; Rodrigue, D. *Proc ANTEC* **2005**, 1346.
12. Pommet, M.; Juntaro, J.; Heng, J. Y. Y.; Mantalaris, A.; Lee, A. F.; Wilson, K.; Kalinka, G.; Shaffer, M. S. P.; Bismarck, A. *Biomacromolecules* **2008,** *9*, 1643.
13. Bessadok, A.; Langevin, D.; Gouanve, F.; Chappey, C.; Roudesli, S.; Marais, S. *Carbohydr. Polym.* **2009,** *76*, 74.
14. Thamae, T.; Baillie, C. *Compos. Interface* **2007,** *14*, 821.
15. Tronc, E.; Hernandez-Escobar, C. A.; Ibarra-Gomez, R.; Estrada-Monje, A.; Navarrete-Bolanos, J.; Zaragoza-Contreras, E. A. *Carbohydr. Polym.* **2007,** *67*, 245.
16. Nishino, T.; Matsuda, I.; Hirao, K. *Macromolecules* **2004,** *7*, 7683.
17. Cassano, R.; Trombino, S.; Bloise, E.; Muzzalupo, R.; Iemma, F.; Chidichimo, G.; Picci, N. *J. Agr. Food. Chem.* **2007,** *55*, 9489.
18. Fair, M. K. C.; Diwan, S. M.; Thomas, S. *J. Appl. Polym. Sci.* **1996,** *60*, 1483.
19. Ishida, H.; Bussi, P. *Macromolecules* **1991,** *24*, 3569.
20. Niak, J. B.; Mishra, S. *Polym.-Plast. Technol.* **2005,** *44*, 687.
21. Estrada-Núñez, S. A.; González-Núñez, R.; Rodrigue, D. *Cell Polym.* **2006,** *25*, 277.
22. Tovar-Cisneros, C.; González-Núñez, R.; Rodrigue, D. *J. Cell. Plast.* **2008,** *44*, 223.
23. Doroudiani, S.; Kortschot, M. T. *J. Thermoplast. Compos.* **2004,** *17*, 13.
24. Rizvi, G.; Matuana, L. M.; Park, C. B. *Polym. Eng. Sci.* **2000,** *40*, 2124.
25. Mihai, M.; Huneault, M. A.; Favis, B. D. *J. Cell. Plast.* **2007,** *43*, 215.
26. Michael, R. Polymeric Materials in Organic Synthesis and Catalysis; Buchmeiser: Wiley: New York, **2003.**
27. Socrates G. Infrared and Raman Characteristic Group Frequencies: Tables and Charts, 3rd ed.; Wiley: England, **2004.**
28. Rodrigue, D.; Souici, S.; Twite-Kabamba, E. *J. Vinyl. Addit. Technol.* **2006,** *12*, 19.
29. Annapragada, K. S.; Banerjee, S. *Ind. Eng. Chem. Res.* **2009,** *48*, 3855.
30. Balam Cocom, R. J.; Duarte Aranda, S.; Canche Escamilla, G. *Rev. Mex. Ing. Quím.* **2006,** *5*, 39.
31. Murugan, P.; Mahinpey, N.; Johnson, K. E.; Wilson, M. *Energ. Fuel.* **2008,** *22*, 2720.
32. Chuan-Fu, L.; Jun-Li, R.; Feng, X.; Jina-Jui, L.; Jin Xia, S.; Run Cang, S. *J. Agr. Food Chem.* **2006,** *54*, 5742.
33. Nair, K. C. M.; Kumar, R. P.; Thomas, S.; Schit, S. C.; Ramamaurthy, K. *Compos Part A* **2000,** *31*, 1231.
34. Xu, Y.; Wu, Q.; Lei, Y.; Yao, F. *Bioresource Technol.* **2010,** *101*, 3280.
35. Gregg, S. J.; Sing, K. S. W. Adsorption, Surface Area and Porosity. 2nd ed.; Academic Press: New York, **1995.**
36. Leofanti, G.; Padovan, M.; Tozzola, G.; Venturelli, B. *Catal. Today* **1998,** *41*, 207.
37. Ikem, V. O.; Menner, A.; Bismarck, A. *Langmuir* **2010,** *26*, 8836.
38. Niekraszewicz, B.; Czarnecki, P. *J. Appl. Polym. Sci.* **2002,** *86*, 907.
39. Joseph, P. V.; Thomas, K.; Pillai, S.; Prasad, C. K. S.; Groeninckx, V. S.; Sarkissova, M. *Compos. Part A* **2003,** *34*, 253.
40. Amash, A.; Zugenmaier. *Polym. Bull.* **1998,** *40*, 251.
41. Torres, F. J.; Civalleri, B.; Pisani, C.; Musto, P.; Albunia, A. R.; Guerra, G. *J. Phys. Chem. B* **2007,** *111*, 6327.
42. Kellar, E. J. C.; Evans, A. M.; Knowles, J.; Galiotis, C.; Adrews, E. H. *Macromolecules* **1997,** *30*, 2400.
43. Kellar, E. J. C.; Galiotis, C.; Adrews, E. H. *Macromolecules* **1996,** *29*, 3515.
44. Ishida, H.; Bussi, P. *Macromolecules* **1991,** *24*, 3569.
45. Sun, X.; Li, H.; Zhang, X.; Wang, J.; Wang, D.; Yan, S. *Macromolecules* **2006,** *39*, 1087.
46. Mishra, S.; Verma, J. *J. Appl. Polym. Sci.* **2006,** *101*, 2530.
47. Tajvidi, M.; Najafi, S. K.; Moteei, N. *J. Appl. Polym. Sci.* **2006,** *99*, 2199.
48. Cranks, J. The Mathematics of Diffusion; Oxford University Press: London, Chapter IV, **1975.**
49. Rao, R. M. V. G. K.; Balasubramanian, N.; Manas, C. *J. Reinf. Plast. Comp.* **1984,** *3*, 232.
50. Alvarez, V. A.; Ruscekaite, R. A.; Vazquez, A. *J. Compos. Mater.* **2003,** *37*, 1575.
51. Morcovich, N. E.; Roboredo, M. M.; Aranguran, M. I. *Polymer* **1999,** *40*, 7313.
52. Wang, W.; Sain, M.; Cooper, P. A. *Compos. Sci. Technol.* **2006,** *66*, 379.